Desalination and Water Treatment
www.deswater.com

doi:10.5004/dwt.2018.22113

107 (2018) 285–295
March

pH-independent preconcentration of Hg (II) ions and rapid adsorption of methylene blue in fish and water samples by nano composite of MoS_2@ MWCNT hybrid as a solid phase extraction sorbent

Mohammad Javad Aghagoli[a], Farzaneh Shemirani[b,*]

[a]*School of Chemistry,University College of Science, University of Tehran, P.O. Box 14155-6455, Tehran, Iran, email: j.aghagoli@ut.ac.ir (M.J. Aghagoli)*
[b]*Department of Analytical Chemistry, University College of Science, University of Tehran, P.O. Box 14155-6455, Tehran, Iran, email: shemiran@khayam.ut.ac.ir(F. Shemirani)*

Received 1 September 2017; Accepted 26 February 2018

ABSTRACT

There are a large number sulphur functional groups on the surface of MoS_2 nano sheets. But, the main problem was its hard collection from aqueous solutions owing to relatively high dispersibility in the media. Fabrication of hybrid from MoS_2 can solve this defect. MoS_2 nano sheets were synthesised on surfaces of MWCNT with the hydrothermal method and characterised by X-ray diffraction, energy-dispersive X-ray, field emission scanning electron microscopy and Raman spectroscopy. In addition, solve the problem of collection; adsorption capacity of adsorbent was strengthened. The hybrid was employed for methylene blue (MB) adsorption in river water and Hg (II) preconcentration in canned tuna fish and water samples. Hg (II) with using ICP-OES. Results showed that equilibrium time both analytes was fast. Qua it was 2 min for the Hg (II) and 5 min for MB. In both analytes, the adsorption isotherm and kinetic were better described by Freundlich isotherm and pseudo-second-order kinetic model, respectively. Maximum adsorption was 256.4 mg g^{-1} and 1250 mg g^{-1} for MB and Hg (II), respectively. Adsorbed methylene blue and Hg (II) has been released from the sorbent surface with 0.5 mol L^{-1} ethanol/HNO_3 and sodium thiosulfate (1.0 mol L^{-1}), respectively.

Keywords: Layered sorbet; Kinetic; Thermodynamic; ICP-AES

1. Introduction

Nowadays, heavy metals and organic pollution attract scientists' attention, due to their serious harms to human life. The contamination of natural waters by this pollution is increasingly becoming a basic environmental problem throughout the world, since the pollutants can cause many disorders in the plant and animals and tend to hoard in food chains [1]. Organic dyes, pigments and their related compounds are widely used for many industries, such as paper, textile, wood and food industries. Methylene blue (MB) has wide applications, which include paper coloring, cotton and wool, silks dyeing and as temporary hair colorant [2,3]. Although MB is not a strongly hazardous material, it can cause a series of physiological response, such as heart rate increasing, vomiting, shock, cyanosis and jaundice in humans [4]. Many sorbents such as MG@m-SiO_2 composite [5], hybrid multi wall carbon nano tube-Laponite [6], oxalic acid modified rice Hull [7] and GO/MgO nano composite [8] have applied for the removal of MB from the water. Hg (II) is considered to be an extremely toxic compound which can cause central nervous system disorders, kidney harm, mental deterioration and even death. Due to its bioaccumulation abilities, Hg (II) at trace levels is harmful to human health [9]. Therefore, preconcentration of Hg (II) in food and drinking water samples and controlling of it have become important [10–12].

Layered transition-metal dichalcogenides (TMDC) have widely used as catalyst and biosensor, due to their unique structure [13]. MoS_2 is a family member of layered TMDC that has drawn the attention of many researchers [14]. MoS_2 has a sandwich like layered structure, where each layer is

*Corresponding author.

constructed by covalently bonded groups of three planes; one Mo layer is placed between two S layers [15]. There have many studies on this compound through suitable properties for the diversity of applications, such as electronic devices, energy storage and optical identification [16]. Also, former researchers have indicated that MoS_2 has the potential performance for the adsorption of sulphur compounds and doxycycline [17,18], due to its high adsorption capacity, environmentally friendly and chemically inert [19]. However, due to small sheets of MoS_2 and ability hydrogen bond formation with water, MoS_2 has relatively high dispersibility and hydrophilicity and these features have limited its application as solid phase extraction (SPE) sorbent. To solve these drawbacks, one suggestion is that hybridbe fabricated with carbon nano materials such as multi wall carbon nano tubes.

Carbon-based materials, especially multi wall carbon nano tubes (MWCNT), have attracted more attention because of its small size, large specific surface area and hollow structures. MWCNT could be used as an adsorbent for the adsorption of organic dyes [20], heavy metal [21] and organic compounds [22]. However, the adsorption performances of MWCNT for the pollutants are not satisfactory, possibly due to the serious aggregation of MWCNT, poor interaction between it with adsorbate and limited availability of active sites on its surfaces. Thus, many efforts have made to design and synthesize novel types of composite based on MWCNT with organic and inorganic materials. The resulting composite materials would integrate the properties and advantages of each component and make the composites exhibit synergic or complementary performances [23–26]. Therefore, surface modification of MWCNT using various species would combine the properties and advantages of both them and greatly improve the functionalities and properties. Hence, it is expected that from combining MoS_2 and MWCNT, an attractive sorbent be provided with high adsorption capacity and be separable with ordinary centrifuges in aqueous media. Surfaces with a negative charge of MoS_2 react with edges and surfaces of MWCNT through π–stacking interaction, consequently forms a chemical bond between MWCNT and MoS_2. As a result, MoS_2@MWCNT can enhance the adsorption properties compared to the MoS_2.

The applications of MoS_2@MWCNT are being increased. Study of previous works indicates that performance of MoS_2@MWCNT hybrid was investigated in various fields such as electrode materials for lithium batteries, components of solar cells, and highly active and stable electro catalysts for production of hydrogen from water [27,28]. Despite their potential advantages, special attention hasn't paid to the SPE application of this hybrid for adsorption of various analytes, till now. Metal ions and dyes on the hybrid adsorb via electrostatic interactions between edges and surfaces of MoS_2 nano sheets deployed on MWCNT and target species.

In this work, we synthesised MoS_2@MWCNT hybrid by a simple hydrothermal method and then used for adsorption of MB in river water and preconcentration of Hg (II) in canned tuna fish, river water and tap water samples. The effect of several variables such as pH, contact time, eluent type and potentially interfering ions were investigated in a batch system. The results showed that the hybrid has high adsorption capacity for fast adsorption of MB and ultrafast preconcentration of Hg (II).Also, adsorption isotherm, kinetic and thermodynamic studies were performed.

2. Experimental

2.1. Materials and instruments

Multi wall carbon nano tubes (MWCNT) were purchased from the research institute of Petroleum Industry (Tehran, Iran). The MWCNT has lengths of 5–15 μm and outer diameters of 10–20 nm with purities greater than 90% claimed by the manufacturer. Sodium molybdate dehydrate and potassium thiocyanate was obtained from Sigma-Aldrich (USA). Methylene Blue was purchased from Sigma (Germany). A standard stock solution of Hg(II) (1000 mg L^{-1}) was prepared by dissolving spectral pure-grade $HgCl_2$ in deionised water with the addition of diluted hydrochloric acid. The pH adjustment for adsorption experimental was performed with 0.1 mol L^{-1} of HNO_3 and 0.1 mol L^{-1} NH_3.

The morphology and composition of the hybrid were analyzed with a field emission scanning electron microscope (FESEM, model S-4160, Hitachi, Japan) which was equipped with an energy-dispersive X-ray analyzer (EDX). For X-ray diffraction (XRD) measurement, a Shimadzu 7000 S X-ray diffract meter with Cu-Kα (λ = 1.54 Å) radiation in the 2θ range of 10–80° was used. Also, Raman spectra were measured with a Raman microscope (Renishaw, England). For the Hg (II) determination an IRIS Advantage ER-S inductively coupled plasma atomic emission spectrometer (TJA, USA) (RF power supply: 1.15 kW; Ar carrier gas flow rate: 0.6 L min^{-1}; Ar auxiliary gas flow rate: 1.0 L min^{-1}; Ar coolant gas flow rate: 14.0 L min^{-1}; viewing height: 15 mm; wavelength of Hg: 194.227 nm) was employed. Also, the dye concentrations were determined using a UV-vis spectrophotometer (Lambda–25 UV–visible, λ_{max} = 665 nm). The refrigerated centrifuge (Hettich, 320 R, Kirchlengern, Germany) was used for centrifuge of solutions and samples that were adjusted pH by pH meter (Metrohm, model-692, Switzerland, Swiss).

2.2. Synthesis of MoS_2@MWCNT hybrid

The MoS_2@MWCNT hybrid was fabricated by a hydrothermal method as follows [29]. First, 0.1 g of MWCNT was dispersed in 60 mL deionised water by ultra sonication for 5 h. Then 0.3 g $Na_2MoO_4{\cdot}2H_2O$ and after several minutes 0.8 g KSCN was added to the suspension. The mixture was transferred into a 100 mL Teflon-lined stainless steel autoclave which was heated to 200°C for 24 h. After cooling to room temperature, the black precipitates were collected by centrifugation and washed with deionised water and ethanol and dried in an oven at 80°C to obtain the hybrid. Synthetic MoS_2@MWCNT is schematically illustrated in Fig. 1.

2.3. Sample preparation

Shilaneh canned tuna fish sample purchased from popular supermarket in Tehran, Iran and its contents homogenized thoroughly in a mixer. Then, the mixture digested according to the following procedure: 2.0 g homogenized sample was placed in a 100 mL beaker and 10 mL of concentrated HNO_3 (65% w/w) and 5.0 mL of H_2SO_4 (98% w/w) was added drop wise to the beaker. The beaker was placed on a steam bath to complete dissolution. Then the solution was transferred into a 50 mL volumetric flask and placed under the extraction process to the determination of Hg (II)

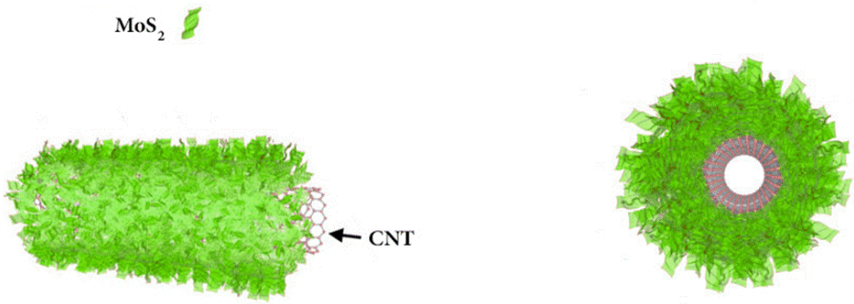

Fig. 1. MoS_2@MWCNT. hybrid.

in the digested sample with ICP-AES. Water samples were collected from 15 Khordad river (Qom, Iran) and tap water (Tehran, Iran), acidified with 5.0 mL of diluted nitric acid and filtered through a filter paper (Whatman No. 40) to remove particles and stored at 4°C.

2.4. Adsorption experiments

The adsorption of MB and preconcentration of Hg (II) on MoS_2@MWCNT hybrid were studied to find the optimum pH, adsorbent dosage and contact time for each analyte by using the batch technique. The hybrid can be well-dispersed in the aqueous solutions, as well as adsorbed MB and Hg(II).

The MB adsorption experiments have performed in 25 mL of a sample solution containing 1.0 mg L^{-1} of MB. After addition 20 mg of the adsorbent and adjustment of pH at 8, the color of the solution turned from light blue to color less within 5 min shaking. Then, the hybrid was separated by centrifuging of suspensions at 5000 rpm for 5 min and MB concentrations were measured by UV-visible spectrophotometer at 665 nm.

The preconcentration procedure of Hg (II) was consisted of two steps: First, 25 mL of sample solution containing 100 µg L^{-1} Hg (II) was transferred to a 50 mL conical flask; without need to pH adjustment, the solution was shaking for 2 min to facilitate adsorption of the Hg (II) on the MoS_2@MWCNT (15 mg). Subsequently, the solution was centrifuged and the adsorbent was collected. In desorption step, the adsorbed Hg (II) were eluted with 2 mL of sodium thiosulfate 1 mol L^{-1} for 1 min. Finally, the hybrid was collected, and the eluent was transferred into a test tube for the determination of desorbed Hg (II) concentration by ICP-AES.

3. Results and discussion

3.1. Characterisation

Raman spectroscopy was applied to investigate structures of MoS_2 and MoS_2-MWCNT. As can be seen in Fig. 2, the appearance of two peaks at 340 and 408 cm^{-1} are related to the E^1_{2g} and A_{1g} vibrational mode of MoS_2, respectively. E^1_{2g} and A_{1g} correspond with atom dislocation which isorthogonal to each other, in which E^1_{2g} involves in-layer displacements of S and Mo while A_{1g} involves out of layer symmetric displacement of S along the c-axis (Fig. 3) [30]. The structure

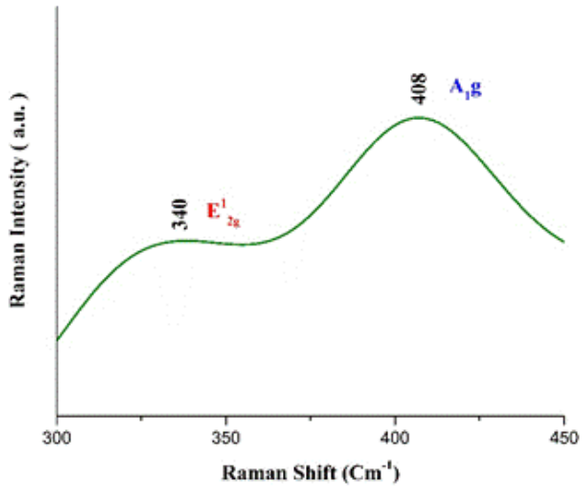

Fig. 2. Raman spectrum of the E^1_{2g} and A_{1g} vibrational modes.

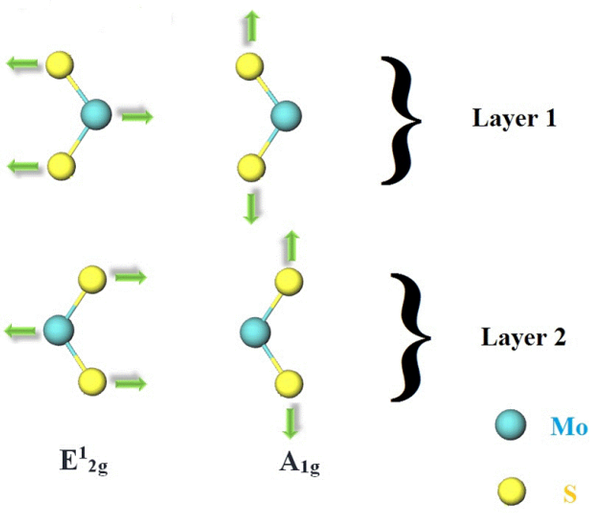

Fig. 3. Atomic displacement of the E^1_{2g} and A_{1g} vibrational modes in bulk MoS_2.

of MoS_2 may contain vital defect sites due to larger E^1_{2g} peak width and the weaker intensity. At these defect sites it is assumed that there are many structurally and coordinately unsaturated S. The Raman spectrum of MWCNT reveals D band at 1350 cm^{-1} and G band at 1585 cm^{-1} that D band corresponded to scattering from disorders or local defects present in the MWCNT and G band corresponded to the in-plane tangential stretching of the C-C bonds. For a MoS_2@MWCNT hybrid, it is clear that besides the typical D band and G band of MWCNT, there are two additional significant peaks of MoS_2 that correspond to the E^1_{2g} and A_{1g} modes (Fig. 4a) [31]. Fig. 4b represents the XRD patterns of MoS_2 and MoS_2-MWCNT hybrid. In the XRD pattern of MoS_2, the peaks at 34° (100), 40° (103) and 58° (110) are attributed to the MoS_2 structure. The XRD pattern of the MoS_2@MWCNT hybrid included all diffraction peaks related to the MoS_2, furthermore, peaks around 25° related to the (002) plane of the MWCNT was observed. For the hybrid of MoS_2@MWCNT hybrid, the peak from the contribution of MWCNT locates at 25°, which is very similar to MWCNT, it shows MoS_2

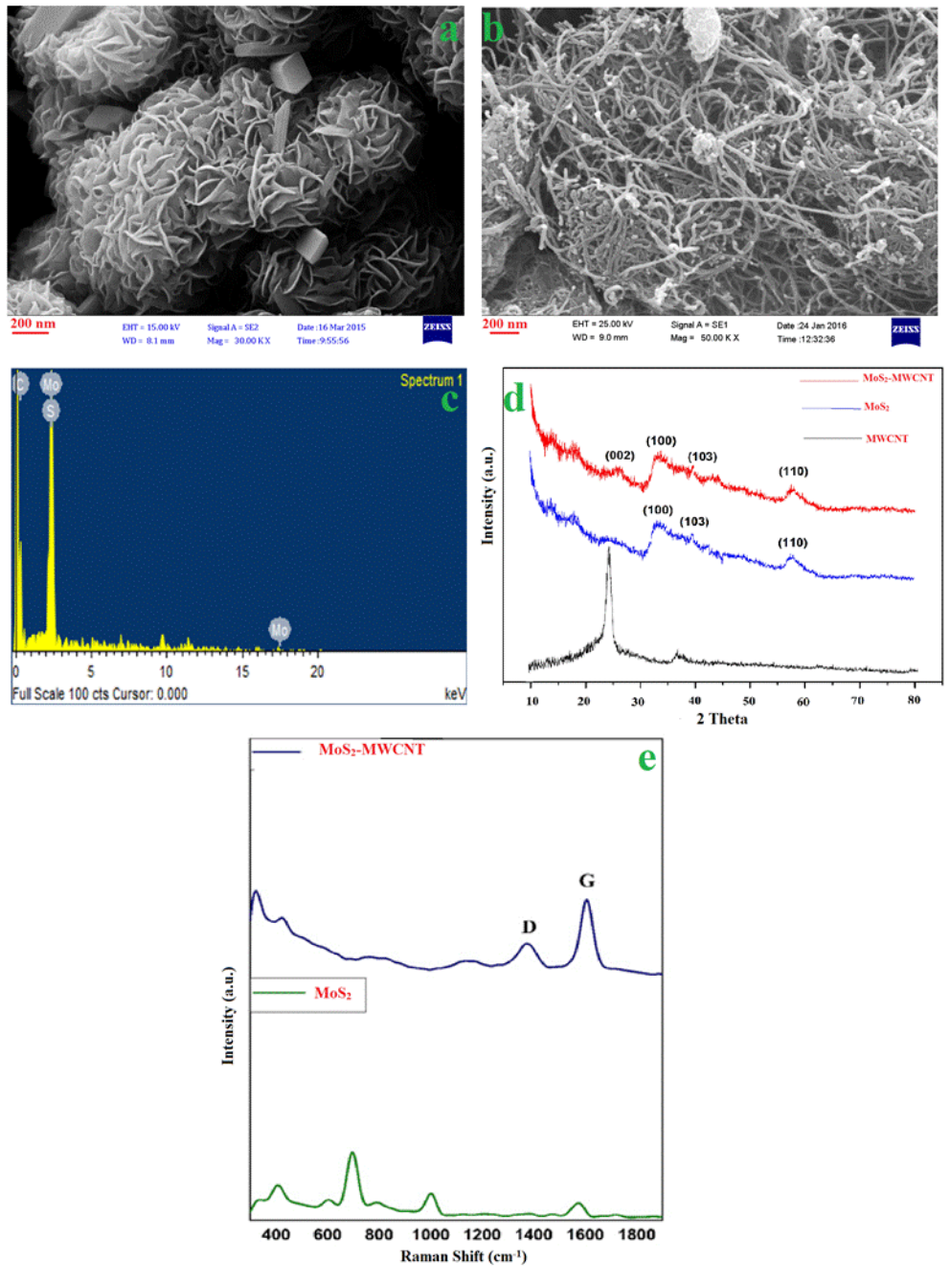

Fig. 4. FESEM (a, b), EDX(c), XRD patterns (d) and Raman spectra (e) of MoS_2 and MoS_2@MWCNT.

outer shells do not introduce much distortion to MWCNT surface [32]. Fig. 4c and d show the FESEM images of the MoS_2 nano sheets and MoS_2@MWCNT hybrid. Fig. 4c shows the FESEM image of the MoS_2, illustrating a 3D sphere-like architecture. Also, MoS_2 nano sheets were well dispersed on the surfaces of MWCNT (Fig. 4d). This structure is helpful to increase the surface areas of the hybrid. The energy-dispersive X-ray (EDX) mapping analysis further proves the good distribution of MoS_2@MWCNT (Fig. 4e).

3.2. Effect of pH

In order to investigate the influence of pH on the performance of the hybrid for adsorption of MB and Hg (II), it was selected a range of pH from 2 to 10, while concentrations of MB and Hg (II) were 1.0 and 0.1 mg L^{-1}. Also, adsorbent dosage was 20 mg for MB and 15 mg for Hg (II) and the samples were individually shaken for a certain time. Then the samples were centrifuged at 5000 rpm for 5 min at room temperature to separate the hybrid from solution. Fig. 5a shows the effect of sample pH on recoveries of Hg (II) (red bar) and removal of MB (blue bar). As can be seen, there was no significant dependence between Hg (II) recovery and changes of pH, so that despite changes of pH from acidic conditions to alkaline, the recoveries of Hg (II) were more than 95%, continually. Therefore, the extraction of Hg (II) by the hybrid didn't need to adjustment of the solution's pH, and the hybrid can be used for Hg (II) adsorption in any pH with excellent performance. The results for the effect of pH on adsorption the Hg (II) can be described on the basis of hard and soft acid-base theory. Hg (II) ions have a high affinity for self-assembly with functional groups of sulphur. Affinity as donor atoms is according to O < N < S. MoS_2 compound contains a large number of sulphur groups which are able to react with various metal ions like Hg(II). Interaction of Hg (II) with MoS_2 resulted in chemisorption of Hg (II) through unreconstructed surfaces and hollow, bridge, or intermediate sites, since these structures are energetically favored for chemisorption. Moreover, the excellent interaction of Hg (II) with the surface of the hybrid, particularly, in acidic media can relate be to two main mechanisms of ion exchange between adsorbed hydrogen ions on surfaces of the hybrid and the target ions and also the electrostatic interaction between the metal ions and hybrid. It should also be noted that the high uptake rate may be owing to the availability of a large number of active sites for adsorption of Hg (II), because Hg-S forms a complex through occupancy of Hg (II)'s empty orbitals by free paired electrons in the S structure.

Also, it is clear in Fig. 5a that removal percentage of MB increased from 23% to 88%, while pH increased from 2 to 7, then the removal (%) remained constant in range 7.5–8.5 and finally reduced from pH 9 to 10. So, optimised pH was selected 8.0 for adsorption of the MB in subsequent experiments. In severe acidic conditions, the negative charged MoS_2 surfaces are more protonated, and this is the main reason for rejection of MB with positive charged. Therefore, adsorption of MB decreases in acidic solution. With increasing of pH, the number of hydrogen ions in the solution decreases. Consequently, competition between hydrogen ions and MB reduced for adsorbing on active sites of the hybrid.

3.3. Effect of the hybrid dose

The effect of MoS_2@MWCNT hybrid dosage on adsorption of the MB and Hg (II) is shown in Fig. 5b. The removal percentage of MB increased almost linearly from 39.0% to about 90.0% as dosage increases from 5.0 mg to 15.0 mg. When the hybrid dosage increases to 20.0 mg, the adsorption maintains at about 96%, indicating that most of MB were absorbed by the hybrid. Addition of more hybrid had little effect. Accordingly, 20.0 mg of the hybrid was enough for completely react with MB of the sample solution.

Based on the tendency strong interaction between Hg (II) ions and S groups, it was expected the hybrid dosage would not have a significant effect. Fig. 5b confirmed this claim, as can be seen with increasing amount of the hybrid from 5.0 mg to 30.0 mg, recoveries of Hg (II) remained in range 90.6–98.5. Nevertheless, amount of 15.0 mg of MoS_2@MWCNT was selected as optimised the sorbent dosage.

3.4. Effect of contact time

The effect of contact time on the adsorption both analytes was investigated from 1–13 min (Fig. 5c). 25 mL of 1 mg L^{-1} of MB with 20 mg of the hybrid was contacted. After shaking at different times, the absorbance of filtrated dye was measured. The difference of absorbance before and after adsorption showed the percentage of MB removal. It was found that more than 96% removal of MB occurred in the first 5 min and then, adsorption of MB had not significant variation. In fact, exfoliated MoS_2 on surfaces of MWCNT increases the accessible active sites and improves surface area. Thus, shaking time was fast in MB adsorption process. As the sites were filled up, the adsorption percentage didn't show a significant increase. In this step, the kinetics will be more dependent on the rate at which the analyte is transported from the aqueous solution to the active sites of hybrid. Such a fast adsorption rate could be attributed to the external surface adsorption and absence of internal diffusion resistance.

In order to investigate the effect of time on the extraction efficiency, the general procedure was performed for 25 mL of the sample solution, which contains 100 μg L^{-1} of Hg(II). According to the results of Fig. 5c, the recovery of the Hg (II) was high and after 2 min reached to 98%. Initial ultrafast extraction is due to the availability of a large number of functional groups of sulphur in the surface of the hybrid and adsorbent has a high tendency for the sorbate ions.

3.5. Effect of sample volume and foreign ions

In order to obtain high preconcentration factor (PF) in the solid phase extraction of Hg (II), the effect of sample volume was studied and the results are depicted in Fig. 5d. The solutions with concentration 100 μg L^{-1} of Hg (II) contained 15 mg of the hybrid and sample volumes were from 20 to 700 mL. The Hg(II) were recovered well up to 600 mL of sample volume to recovery beyond 95%. The PF was calculated by the ratio of the highest sample volume (600 mL) to the lowest eluent volume (2 mL) and the PF was obtained 300 for Hg (II).

The influences of some cations and anions were researched on the recovery of Hg (II) (Table 1). High con-

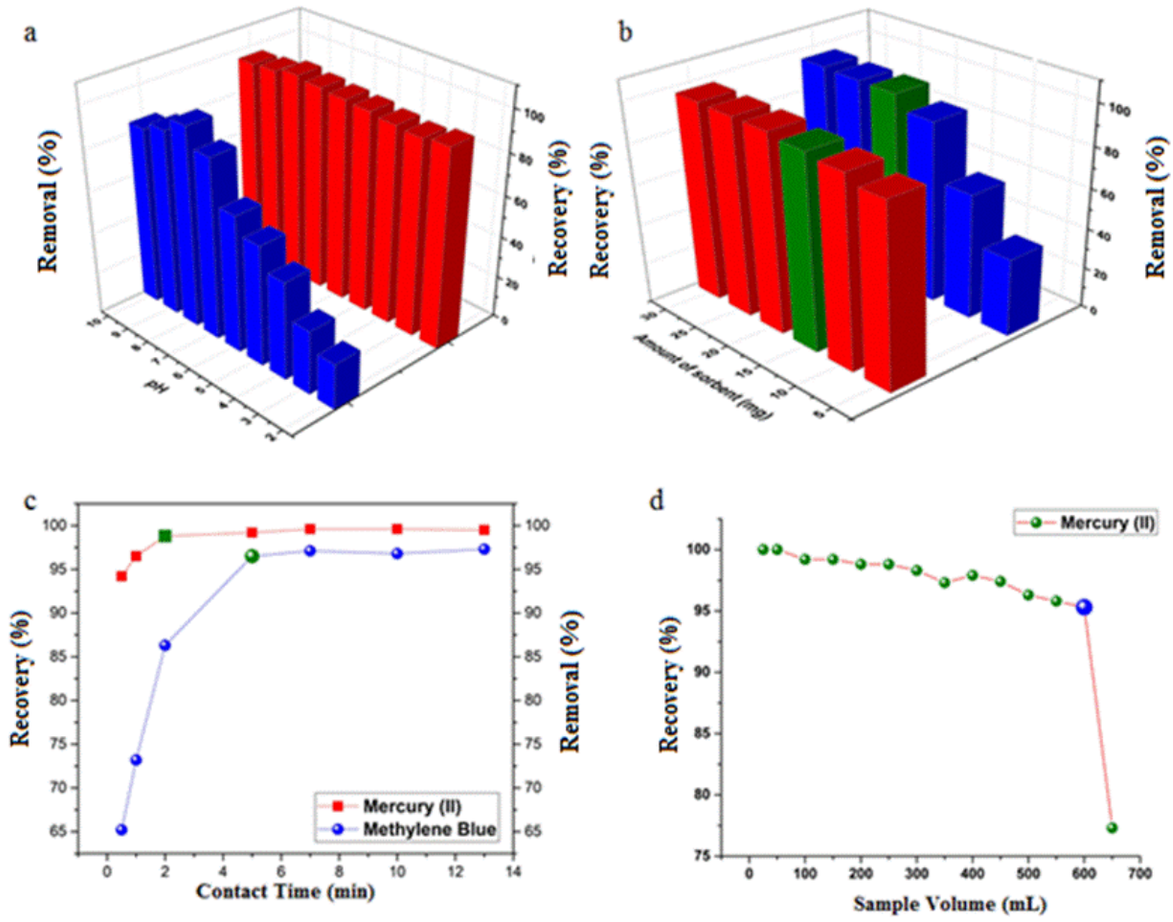

Fig. 5. Effects of (a) pH, (b) amount of sorbent, (c) contact time and (d) sample volume.

centrations of some cations and anions, also some transition metals have not interfered on the determination Hg (II). It is clear that in excess of 100 mg L^{-1} of cations such as K^+, Na^+, Ca^{2+} and Mg^{2+} and 100 mg L^{-1} of anions such as SO_4^{2-}, HPO_4^{2-} and Cl^- and 5 mg L^{-1} of transition metals ions such as Zn (II), Cd(II), Mn(II), Ni(II) and Co(II) haven't significant interfere on the adsorption of Hg (II), when the tolerance limit was set as the number of ions causing recoveries of the examined elements to be less than 95%. Due to the basis of hard and soft acid-base theory and also, more affinity of the functional group of S in the surface of the hybrid to coordinate with Hg (II) in comparison with other metal ions, extraction of Hg (II) clearly improves.

3.6. Kinetic study

In order to understand the characteristics of the adsorption process, the kinetics of MB and Hg(II) adsorption on the MoS_2@MWCNT hybrid were investigated by using four kinetic models, i.e. the pseudo-first-order; pseudo second-order models, Elovich and Weber–Morris intra particle diffusion models. Pseudo-first-order and pseudo-second-order models can be described with following linear equations [33]:

$$\log (q_e - q_t) = \log q_e - k_1 t/2.303 \quad (1)$$

$$t/q_t = 1/k_2 q_e^2 + t/q_e \quad (2)$$

where q_e and q_t (mg g^{-1}) represent the quantity of adsorbed analyte at equilibrium and different times (min), respectively; k_1 (min^{-1}) and k_2 (g mg^{-1} min^{-1}) are the rate constants of pseudo-first-order and pseudo-second-order models, respectively. The kinetic parameters including correlation coefficients (r^2), k_1, k_2 and $q_{e,cal}$ values were determined by linear regression for both analytes and were given in Table 2.

It could be easily observed that the r^2 values (r^2 = 0.992 for MB and r^2 = 0.995 for Hg (II)) of the pseudo-second-order kinetic model were much higher than a pseudo-first-order kinetic model for both analytes. Furthermore, the $q_{e,cal}$ values for the pseudo-second-order were in agreement with that of experimental data ($q_{e,exp}$). These results suggest that the pseudo-second-order can be used to represent the adsorption data and the adsorption process involves chemisorption.

Obviously, the pseudo-second-order kinetic model was more valid to describe the adsorption behavior of both analytes, which was consistent with Table 2. The pseu-

Table 1
Effect of potentially interfering ions on the recovery of 100 µg L^{-1} Hg (II)

Interference	Concentration (mg L^{-1})	R[a] % ± SD[b]
Na^+	20,000	96.1 ± 1.7
K^+	20,000	95.8 ± 2.1
Mg^{2+}	10,000	95.0 ± 2.2
Ca^{2+}	10,000	95.2 ± 1.8
Cu^{2+}	20	95.3 ± 1.8
Fe^{2+}	20	95.7 ± 1.9
Zn^{2+}	20	94.8 ± 1.3
Ni^{2+}	20	95.1 ± 2.4
Pb^{2+}	20	95.2 ± 2.2
Cd^{2+}	20	95.4 ± 2.5
Cr^{3+}	20	96.4 ± 1.6
Fe^{3+}	20	95.1 ± 2.5
NO_3^-	20,000	96.6 ± 1.8
Cl^-	20,000	95.1 ± 2.1
HCO_3^-	2,000	95.3 ± 2.1
CO_3^{2-}	2,000	95.3 ± 1.8

[a]Recovery.
[b]Standard Deviation.

Table 2
The data of pseudo-first-order, pseudo-second-order, Elovich and Weber–Morris intra particle diffusion models constants for the adsorption of MB and Hg(II) on MoS_2@MWCNT hybrid

Kinetic models	Kinetic parameters	MB	Hg(II)
Pseudo-first-order	k_1 (min^{-1})	0.2668	1.0566
	$q_{e,cal}$ (mg g^{-1})	37.248	119.54
	r^2	0.978	0.963
Pseudo-second-order	k_2(g (mg^{-1} min^{-1}))	0.0200	0.0139
	$q_{e,cal}$ (mg g^{-1})	50.251	147.05
	r^2	0.992	0.995
Elovich	α (mg g^{-1} min^{-1})	134.35	1082.71
	β (g mg^{-1})	0.1038	0.0339
	r^2	0.955	0.981
Weber–Morris	k_{id} (mg g^{-1} min^{-1})	11.329	44.814
	C	13.678	58.633
	r^2	0.980	0.980
$q_{e,exp}$ (mg g^{-1})		51.25	145.00

do-second-order kinetic model includes every four steps of adsorption. These steps as follow: (1) adsorbate transport from the bulk solution to the adsorbent surface; (2) diffusion through the boundary layer on the solid's surface (film diffusion); (3) adsorption on active sites; (4) intra-particle diffusion into the interior of the adsorbent [34]. Generally, steps 2 and step 3 are considered to be the rate-limiting step. The Elovich [35] and Weber–Morris intra particle diffusion [36] models were applied in order to investigate the diffusion mechanism. The equations of the models are as follows:

$$q_t = 1/\beta\ (\alpha\ \beta) + 1/\beta \ln t \quad (3)$$

$$q_t = k_i t^{1/2} + C \quad (4)$$

where α is the initial adsorption rate (mg g^{-1} min^{-1}), β is the desorption constant (g mg^{-1}) which are calculated from intercept and slope of plot q_t versus ln t. The plot of q_t versus ln(t) should yield a linear relationship with a slope and intercept of (1/β) and (1/β) ln (α β), respectively. The k_i (mg g^{-1} $min^{1/2}$) was the rate constant of intra particle diffusion, C (mg g^{-1}) is the thickness of boundary layer (the larger the intercept, the greater the boundary layer effect will be).

The Elovich constants obtained from the slope and the intercept of the straight line [37] and were reported in Table 2. The general explanations for this form of kinetic equation involve variations of the energy of chemisorption, in which the active sites are heterogeneous in the hybrid. This supports the fact that the heterogeneous sorption mechanism is likely responsible for uptake both analytes. The Elovich model basically supports chemisorption. The correlation coefficients (r^2) values of Elovich model for both analytes were included the following: 0.955 and 0.981 for MB and Hg (II), respectively. In general, the r^2 values for the hybrid show the lack of success for the Elovich model.

When the linear plot of q_t versus $t^{1/2}$ passes through the origin, intra particle diffusion mechanism is considered a rate-limiting step for the adsorption process [36]. The corresponding kinetic parameters are listed in Table 2. It was clear that the regression of q_t vs. $t^{1/2}$ was inclined to be linear and the plots did not pass through the origin, suggesting that the intra particle diffusion is not the only rate-controlling step and the film diffusion maybe also significant in the rate-controlling step because of the large intercepts of linear portion of the plots [36].

3.7. Isotherm study

Adsorption isotherms studies give useful information about the adsorption capacity of sorbent. In this study, four well-known models include the Langmuir, Freundlich, Temkin and Dubinin-Radushkevich isotherms were selected. The theoretical of Langmuir isotherm is based on the assumption of a mono layer adsorption, where all the sorption sites are identical and energetically equivalent [38].While the Freundlich model is based on multilayer adsorption on the heterogeneous surface [39]. Also, Temkin isotherm investigates the heat of adsorption and the adsorbate-adsorbate interactions [40]. Dubinin-Radushkevich is generally applied to express the adsorption process occurring on both homogeneous and heterogeneous surfaces[41]. The adsorption experiments were carried out at initial concentration 10–350 mg L^{-1} for MB and 10–1700 mg L^{-1} for Hg (II). The linear forms of the four isotherms are given by the following equations:

$$C_e/q_e = 1/q_{max} K_L + 1/q_{max} C_e \quad (5)$$

$$\log q_e = \log K_F + 1/n \log C \quad (6)$$

$$q_e = \beta \ln\alpha + \beta \ln C_e \quad (7)$$

$$q_e = q_s \exp(-\beta \varepsilon^2) \quad (8)$$

where C_e (mg L^{-1}) is the equilibrium concentration, q_e (mg g^{-1}) is the amount of adsorbed analyte at equilibrium time, q_{max}(mg g^{-1}) is the maximum amount of the adsorbate per unit weight of sorbent for complete mono layer coverage capacity and K_L (L mg^{-1})is the adsorption rate. Values of q_{max} and K_L are determined from the linear regression plot of (C_e q_e^{-1}) vs. C_e. K_F and n are Freundlich constants. K_F represents the capacity of the adsorbent for the adsorbate, and *1/n* shows adsorption intensity of analyte on the adsorbent, which is a function of the strength of adsorption. A linear regression plot of log q_e versus log C_e gives K_F and n values. Parameters of α (L g^{-1}) and β (J mol^{-1}) are the Temkin constants related to the binding equilibrium isotherm and to the heat of adsorption, respectively. Amounts of α and β are calculated from the slope and intercept of q_e vs. ln C_e. Factor ε is the Polanyi potential constant, β is the adsorption energy constant (mol^2 kJ^{-2}), q_s is the theoretical isotherm saturation capacity (mg g^{-1}). Table 3 summarized the values of Langmuir, Freundlich, Temkin and Dubinin-Radushkevich models for the adsorption of MB and Hg (II) constants with coefficients. Regression correlation coefficient of Freundlich model was greater than that obtained from Langmuir isotherm which pointed out that Freundlich isotherm model more fit for MB and Hg (II). The results suggest that adsorption of both analytes is accompanied by multilayer formation. The values of Temkin constants are given in Table 3, too. The adsorption energies obtained for adsorption of MB and Hg (II) on the hybrid were 38.65 and 195.0 J mol^{-1}, respectively. These values indicate that the adsorption process is endothermic and also account for the strong interaction between MoS_2@MWCNT hybrid and both analytes. The high value for adsorption energy in case of Hg(II) compared to that of MB can be attributed to the low value of its r^2. Also, obtained results from Dubinin-Radushkevich model are presented in Table 3. The values of q_s and β were calculated from the intercept and slope of the ln q_e versus ε^2.

Table 3
MB and Hg(II) adsorption constants by MoS_2@MWCNT hybrid in aqueous solution based on the Langmuir, Freundlich, Temkin and Dubinin-Radushkevich adsorption models

Adsorption isotherms	Isotherm constants	MB	Hg(II)
Langmuir	K_L (L mg^{-1})	0.0319	0.0116
	q_{max} (mg g^{-1})	256.4	1250
	r^2	0.964	0.988
Freundlich	K_F (L mg^{-1})	1.7873	2.3588
	N	1.1767	1.1385
	r^2	0.994	0.996
Temkin	α (L g^{-1})	1.0624	2.0897
	β (J mol^{-1})	38.65	195.0
	r^2	0.898	0.873
Dubinin–Radushkevich	q_s (mg g^{-1})	121.5	320.217
	β (mol^2 kJ^{-2})	4.8×10^{-8}	0.013
	r^2	0.650	0.632

3.8. Thermodynamic study

The thermodynamic parameters were evaluated to confirm the nature of the adsorption and the inherent energetic changes involved during adsorption of analytes. Standard enthalpy (ΔH°), free energy (ΔG°) and entropy changes (ΔS°) were calculated to determine the thermodynamic feasibility and the spontaneous nature of the process. Therefore, the values of ΔH° and ΔS° were obtained from the slope and intercept of the ln K_d versus 1/T curve according to Eq. (9):

$$ln\ K_d = \left(\frac{\Delta S^\circ}{R}\right) - \left(\frac{\Delta H^\circ}{R}\right)\frac{1}{T} \quad (9)$$

where K_d (L g^{-1}) is the distribution coefficient ($K_d = C_{ads}\ C_e^{-1}$), T (K) is the adsorption temperature and R (8.314 J mol^{-1} K^{-1}) is the universal gas constant. Moreover, C_{ads} (mg L^{-1}) is the amount of lead and nickel adsorbed on sorbent at equilibrium, and C_e (mg L^{-1}) is the equilibrium concentration of target analytes in solution [42]. The ΔG° value of can be determined from:

$$\Delta G^\circ = \Delta H^\circ - T\Delta S^\circ \quad (10)$$

As can be seen in Table 4, the ΔG° values are negative for all temperatures, indicating that MB and Hg (II) adsorbed spontaneously on MoS_2@MWCNT hybrid and that the system does not gain energy from an external source.

Moreover, the value of free energy became more negative with raise in temperature suggesting that the adsorption became more favorable at higher temperatures. The positive values of S and H indicate that the adsorption process is endothermic with an increase in the degree of randomness of the system.

3.9. Desorption and reusability

According to results for effect of pH, the adsorption of MB was not efficient in the acidic condition. Therefore, elution with the acidic solution may be favorable. According to this, different concentrations of methanol/HNO_3 and ethanol/HNO_3 (0.1 M, 0.3 M and 0.5 M in volume of 2 mL) were employed to reuse the hybrid. It was observed that with the increase in ethanol/HNO_3 concentration from 0.1 mol L^{-1} to 0.5 mol L^{-1} the release of MB increased from 86% to 99%. Hence, 0.5 mol L^{-1} ethanol/HNO_3 was employed for desorption of MB. Hg (II) elution from the hybrid surface was also examined using 2 mL various concentrations (0.1 M, 0.5 M and 1.0 M) of thiourea, L-cysteine and sodium thiosulfate as eluent. The obtained results showed (Table 5) that 2 mL of

Table 4
The thermodynamic data for MB and Hg (II) adsorption using as MoS_2 nano sheets-MWCNT hybrid

Analyte	ΔG° (kJ mol)			ΔH° (kJ mol^{-1})	ΔS° (J $K^{-1}mol^{-1}$)
	298K	308K	321K		
MB	3.7686	4.2843	4.9117	+11.1848	+50.170
Hg(II)	4.7073	5.1754	5.6904	+7.9656	+42.580

Table 5
Elution of adsorbed MB and Hg(II) from MoS_2 nano sheets MWCNT hybrid

Analyte	Eluent[a]	Concentration	R (%)
MB	Methanol/HNO_3	0.1	74
		0.3	82
		0.5	88
	Ethanol/HNO_3	0.1	86
		0.3	91
		0.5	99
Hg (II)	Thiuorea	0.1	77
		0.5	83
		1.0	88
	L-cysteine	0.1	68
		0.5	77
		1.0	85
	Sodium thiosulfate	0.1	88
		0.5	96
		1.0	99

[a]Eluent volume 2 mL.

sodium thiosulfate 1 mol L^{-1} can release more than 99% of adsorbed Hg (II).

Moreover, in order to evaluate the reusability of the hybrid, it was subjected to several loadings with the sample solution and subsequent elution. It was found that after five cycles of adsorption and desorption, the recovery of both analytes was quantitative (90% ≤) which confirm the efficiency and good stability of the hybrid.

3.10. Figure of merit and real sample analysis

A calibration curve was constructed under the optimised conditions, for the determination of Hg (II) according to the preconcentration procedure. Linearity in the final solution was maintained at 0.07–120 µg L^{-1} with a correlation factor of 0.995 ($A = 9.3 \times 10^{-3}\ C + 6.3 \times 10^{-4}$). The procedure was repeated three times and the relative standard deviation (RSD) for the determination of 100 µg L^{-1} of Hg(II) was found to be 2.1%. The limit of detection (LOD) was calculated as three times the standard deviation of the blank signal (n = 3) with the preconcentration step and was 20 ng L^{-1}. Also, the limit of quantification and the preconcentration factor were 66.67 ng L^{-1} and 300, respectively.

To investigate the environmental applicability of this method and its efficiency for adsorption of MB in the real sample, a river water sample with initial MB concentration of 16.8 mg L^{-1} was analyzed according to the adsorption experiment. It was observed that about 88.3% of the dyewas removed from the sample which confirmed that the efficiency of the method is in good level.

In order to evaluate the efficiency of the hybrid in preconcentration and extraction of Hg (II), in real samples, the developed method is applied to determine Hg (II) in real samples including canned tuna fish, river water and tap water samples. The recovery test was performed by the analysis of the samples spiked with the known amounts of the metal ions. The analytical results, along with the recovery of the spiked samples of this investigation are given in Table 6. The relative recoveries and matrix effects were determined for spiked samples ($n = 3$). Relative recovery was calculated by dividing the analytical signal for a sample spiked before extraction by the signal for an equal concentration sample in the same matrix spiked after extraction. As shown, recoveries for the target analytes ranged from 95.4% to 107.5%. These results indicate lack of matrices effect and good accuracy of the procedure.

Table 6
Determination of Hg(II) ions in real samples

Sample	Added (µg g^{-1})	Found (µg g^{-1})	R %
Canned tuna fish	0	5.3	–
	10	14.8	95
	20	26.1	104
15 khordad river	0	0.71	
	10	11.2	105
	20	19.8	95
Tap water	0	N.D	–
	10	11.8	103
	20	19.6	99

Table 7
Comparison the MB adsorption property of the hybrid with some sorbents

Adsorbent	Adsorption capacity (mg g^{-1})	Equilibrium time (min)	Ref
Carbonized sludge	25.44	250	[43]
PANI NTs[a]	9.21	120	[44]
PProDOT/MnO_2[b]	13.94	120	[45]
Rice husk	40.59	150	[46]
MoS_2@MWCNT	256.4	5	This work

[a]Polyaniline nano tube
[b]poly (3,4-propylenedioxythiophene)/MnO_2 composites (PProDOT/MnO_2)

3.11. Comparison of the proposed method with other methods

The efficiency of the proposed method was evaluated by comparing the obtained results with those of other similar methods reported in the literature and given in Tables 7 (for MB) and 8 (for Hg (II)). There are some parameters like adsorption of capacity, preconcentration factor, limit of detection and precision achieved in the present work that could be well compared to the procedures which have introduced. Unlike other reported methods, the proposed adsorbent did not require any pretreatment step for the extraction process. Furthermore, there is a possibility of extraction of Hg (II) ions as pH-independent from large volumes of sample in lower extraction times in comparison with conventional SPE sorbents.

Generally, it is obvious that the performance of the hybrid is appropriate with respect to improved adsorption

Table 8
Comparison the Hg(II) adsorption property of the hybrid with some sorbents

Adsorbent	LR (mg L^{-1})	DL (mg L^{-1})	PF	AC (mg g^{-1})	Time (min)	Ref
AMT-OCMK-3 [a]	N.R	40	200	44	175	[47]
PANI/GO [b]	–	–	–	80.7	240	[48]
immobilizing creatine on activated carbon	N.R.	0.06	100	49.5	–	[49]
MWCNTs-Fe_3O_4 MNPs-silica-EET [d]	–	–	–	23.04	2	[50]
GO–AMBT [e]	0.2–150	0.1	120	80.0	13	[51]
MoS_2@MWCNT	0.07-120	0.020	300	1250	2	This work

[a]Ordered mesoporous carbon (CMK-3) was synthesized and functionalized with 2-amino-5-mercapto-1,3,4-thiadiazole groups (AMT-OCMK-3)
[b]Three-dimensional composite of polyaniline (PANI) and graphene oxide (GO)
[c]2-(2-oxoethyl) hydrazine carbothioamide modified silica gel (SG-OHC)
[d](Fe_3O_4)/chelating agent 1-(2-ethoxyphenyl)-3-(4-ethoxyphenyl) triazene functionalized multi-walled carbon nanotubes with silica shell
[e] GO functionalized by a new ligand: (1-(p-acetyl phenyl)-3-(o-methyl benzoate) triazene (AMBT)).

capacity for both analytes as well as it showed fast adsorption rate.

4. Conclusion

In a summary, MoS_2@MWCNT hybrid was prepared using a hydrothermal synthetic and then used for preconcentration of Hg (II) and adsorption of methylene blue. The advantages of the proposed method include fast and pH-independent adsorption of Hg (II) ions, rapid and convenient removal operation of MB, enhanced adsorption capacity, reduce of shaking time and separable to ordinary-speed centrifuges. The adsorption capacities of the hybrid at optimum conditions were found to be 256.4 and 1250 mg g^{-1} for MB and Hg (II), respectively. Langmuir isotherm gave a better fit to adsorption isotherms than other models for both analytes. Also, the kinetic studies of Hg (II) and MB on MoS_2@MWCNT were performed and results indicated that adsorption both analytes followed the pseudo-second-order rate.

References

[1] A. Jamali, A.A. Tehrani, F. Shemirani, A. Morsali, Lanthanide metal--organic frameworks as selective micro porous materials for adsorption of heavy metal ions, Dalt. Trans., 45 (2016) 9193–9200.
[2] N. Nasuha, B.H. Hameed, A.T.M. Din, Rejected tea as a potential low-cost adsorbent for the removal of methylene blue, J. Hazard. Mater., 175 (2010) 126–132.
[3] M. Rafatullah, O. Sulaiman, R. Hashim, A. Ahmad, Adsorption of methylene blue on low-cost adsorbents: a review, J. Hazard. Mater., 177 (2010) 70–80.
[4] A.T. Paulino, M.R. Guilherme, A.V. Reis, G.M. Campese, E.C. Muniz, J. Nozaki, Removal of methylene blue dye from an aqueous media using super absorbent hydrogel supported on modified polysaccharide, J. Colloid Interface Sci., 301 (2006) 55–62.
[5] X.-L. Wu, Y. Shi, S. Zhong, H. Lin, J.-R. Chen, Facile synthesis of Fe_3O_4-graphene@ mesoporous SiO_2 nano composites for efficient removal of Methylene Blue, Appl. Surf. Sci., 378 (2016) 80–86.
[6] M. Loginov, N. Lebovka, E. Vorobiev, Hybrid multi walled carbon nano tube- Laponite sorbent for removal of methylene blue from aqueous solutions, J. Colloid Interface Sci., 431 (2014) 241–249.
[7] S.-M. Lee, S.-T. Ong, Oxalic acid modified rice hull as a sorbent for methylene blue removal, APCBEE Procedia. 9 (2014) 165–169.
[8] M. Heidarizad, S.S. Sengör, Synthesis of graphene oxide/magnesium oxide nano composites with high-rate adsorption of methylene blue, J. Mol. Liq., 224 (2016) 607–617.
[9] Z. Li, S. Xia, J. Wang, C. Bian, J. Tong, Determination of trace mercury in water based on N-octylpyridinium ionic liquids preconcentration and stripping voltammetry, J. Hazard. Mater., 301 (2016) 206–213.
[10] W.X. Ma, F. Liu, K.A. Li, W. Chen, S.Y. Tong, Preconcentration, separation and determination of trace Hg (II) in environmental samples with aminopropylbenzoylazo-2-mercaptobenzothiazole bonded to silica gel, Anal. Chim. Acta., 416 (2000) 191–196.
[11] S. Malci, C. Kavakli, A. Tuncel, B. Salih, Selective adsorption, preconcentration and matrix elimination for the determination of Pb (II), Cd (II), Hg (II) and Cr (III) using 1, 5, 9, 13-tetrathiacyclohexadecane-3, 11-diol anchored poly (p-chloromethylstyrene-ethyleneglycoldimethacrylate) microbe, Anal. Chim. Acta., 550 (2005) 24–32.
[12] E.M. Martinis, R.G. Wuilloud, Enhanced spectrophotometric detection of Hg in water samples by surface plasmon resonance of Au nano particles after preconcentration with vortex-assisted liquid-liquid micro extraction, Spectrochim. Acta Part A Mol. Biomol. Spectrosc., 167 (2016) 111–115.
[13] G. Eda, T. Fujita, H. Yamaguchi, D. Voiry, M. Chen, M. Chhowalla, Coherent atomic and electronic heterostructures of single-layer MoS_2, ACS Nano. 6 (2012) 7311–7317.
[14] K.F. Mak, C. Lee, J. Hone, J. Shan, T.F. Heinz, Atomically thin MoS_2: a new direct-gap semiconductor, Phys. Rev. Lett., 105 (2010) 136805.
[15] D. Voiry, M. Salehi, R. Silva, T. Fujita, M. Chen, T. Asefa, V.B. Shenoy, G. Eda, M. Chhowalla, Conducting MoS_2 nano sheets as catalysts for hydrogen evolution reaction, Nano Lett., 13 (2013) 6222–6227.
[16] X. Zhang, B. Luster, A. Church, C. Muratore, A.A. Voevodin, P. Kohli, S. Aouadi, S. Talapatra, Carbon nanotube- MoS_2 composites as solid lubricants, ACS Appl. Mater. Interfaces., 1 (2009) 735–739.
[17] M. Komarneni, A. Sand, U. Burghaus, Adsorption of Thiophene on Inorganic MoS_2 Fullerene-Like Nano particles, Catal. Letters. 129 (2009) 66–70.
[18] Y. Chao, W. Zhu, X. Wu, F. Hou, S. Xun, P. Wu, H. Ji, H. Xu, H. Li, Application of graphene-like layered molybdenum disul-

phide and its excellent adsorption behavior for doxycycline antibiotic, Chem. Eng. J., 243 (2014) 60–67.
[19] V.G. Pol, S.V. Pol, A. Gedanken, Micro to nano conversion: A one-step, environmentally friendly, solid state, bulk fabrication of WS_2 and MoS_2 nanoplates, Cryst. Growth Des., 8 (2008) 1126–1132.
[20] M.S. Derakhshan, O. Moradi, The study of thermodynamics and kinetics methyl orange and malachite green by SWCNTs, SWCNT-COOH and SWCNT-NH 2 as adsorbents from aqueous solution, J. Ind. Eng. Chem., 20 (2014) 3186–3194.
[21] C. Chen, X. Wang, Adsorption of Ni (II) from aqueous solution using oxidized multi wall carbon nano tubes, Ind. Eng. Chem. Res. 45 (2006) 9144–9149.
[22] X. Peng, Y. Li, Z. Luan, Z. Di, H. Wang, B. Tian, Z. Jia, Adsorption of 1, 2-dichlorobenzene from water to carbon nanotubes, Chem. Phys. Lett., 376 (2003) 154–158.
[23] J.-L. Gong, B. Wang, G.-M. Zeng, C.-P. Yang, C.-G. Niu, Q.-Y. Niu, W.-J. Zhou, Y. Liang, Removal of cationic dyes from aqueous solution using magnetic multi-wall carbon nano tube nano composite as adsorbent, J. Hazard. Mater., 164 (2009) 1517–1522.
[24] A.A. Farghali, M. Bahgat, W.M.A. El Rouby, M.H. Khedr, Decoration of MWCNTs with $CoFe_2O_4$ nano particles for methylene blue dye adsorption, J. Solution Chem., 41 (2012) 2209–2225.
[25] M.R. Nabid, R. Sedghi, A. Bagheri, M. Behbahani, M. Taghizadeh, H.A. Oskooie, M.M. Heravi, Preparation and application of poly (2-amino thiophenol)/MWCNTs nano composite for adsorption and separation of cadmium and lead ions via solid phase extraction, J. Hazard. Mater., 203 (2012) 93–100.
[26] S. Chatterjee, M.W. Lee, S.H. Woo, Adsorption of congo red by chitosan hydrogel beads impregnated with carbon nanotubes, Bioresour. Technol., 101 (2010) 1800–1806.
[27] S. Wang, X. Jiang, H. Zheng, H. Wu, S.-J. Kim, C. Feng, Solvo thermal synthesis of MoS_2/carbon nano tube composites with improved electrochemical performance for lithium ion batteries, Nano sci. Nano technol. Lett., 4 (2012) 378–383.
[28] S.-K. Park, S.-H. Yu, S. Woo, B. Quan, D.-C. Lee, M.K. Kim, Y.-E. Sung, Y. Piao, A simple l-cysteine-assisted method for the growth of MoS_2 nano sheets on carbon nano tubes for high-performance lithium ion batteries, Dalt. Trans., 42 (2013) 2399–2405.
[29] X.C. Song, Y.F. Zheng, Y. Zhao, H.Y. Yin, Hydrothermal synthesis and characterization of CNT@ MoS_2 nanotubes, Mater. Lett., 60 (2006) 2346–2348.
[30] Q. Li, E.C. Walter, W.E. der Veer, B.J. Murray, J.T. Newberg, E.W. Bohannan, J.A. Switzer, J.C. Hemminger, R.M. Penner, Molybdenum disulphide nanowires and nanoribbons by electrochemical/chemical synthesis, J. Phys. Chem. B., 109 (2005) 3169–3182.
[31] D. Nasr Esfahani, O. Leenaerts, H. Sahin, B. Partoens, F.M. Peeters, Structural transitions in mono layer MoS_2 by Lithium Adsorption, J. Phys. Chem. C., 119 (2015) 10602–10609.
[32] V.O. Koroteev, A.V. Okotrub, Y.V. Mironov, O.G. Abrosimov, Y.V . Shubin, L.G. Bulusheva, Growth of MoS_2 layers on the surface of multi walled carbon nano tubes, In org. Mater. 43 (2007) 236–239.
[33] Y.-S. Ho, G. McKay, Pseudo-second order model for sorption processes, Process Biochem., 34 (1999) 451–465.
[34] M.K. Dahri, M.R.R. Kooh, L.B.L. Lim, Application of Casuarina equisetifolia needle for the removal of methylene blue and malachite green dyes from aqueous solution, Alexandria Eng. J., 54 (2015) 1253–1263.
[35] S.H. Chien, W.R. Clayton, Application of Elovich equation to the kinetics of phosphate release and sorption in soils, Soil Sci. Soc. Am. J., 4 (1980) 265–268.
[36] W.J. Weber, J.C. Morris, Kinetics of adsorption on carbon from solution, J. Sanit. Eng. Div., 89 (1963) 31–60.
[37] E. Bulut, M. Özacar, I.A. Sengil, Adsorption of malachite green onto bentonite: equilibrium and kinetic studies and process design, Micro porous Meso porous Mater., 115 (2008) 234–246.
[38] I. Langmuir, The adsorption of gases on plane surfaces of glass, mica and platinum., J. Am. Chem. Soc. 40 (1918) 1361–1403.
[39] U. Freundlich, Die adsorption in lusungen, (1906).
[40] M.J. Temkin, V. Pyzhev, Recent modifications to Langmuir isotherms, (1940).
[41] F. Najafi, O. Moradi, M. Rajabi, M. Asif, I. Tyagi, S. Agarwal, V.K. Gupta, Thermodynamics of the adsorption of nickel ions from aqueous phase using graphene oxide and glycine functionalized graphene oxide, J. Mol. Liq., 208 (2015) 106–113.
[42] X. Sun, L. Yang, Q. Li, Z. Liu, T. Dong, H. Liu, Polyethyleneimine-functionalized poly (vinyl alcohol) magnetic micro spheres as a novel adsorbent for rapid removal of Cr (VI) from aqueous solution, Chem. Eng. J., 262 (2015) 101–108.
[43] W.-H. Li, Q.-Y. Yue, B.-Y. Gao, X.-J. Wang, Y.-F. Qi, Y.-Q. Zhao, Y.-J. Li, Preparation of sludge-based activated carbon made from paper mill sewage sludge by steam activation for dye wastewater treatment, Desalination. 278 (2011) 179–185.
[44] M.M. Ayad, A.A. El-Nasr, Adsorption of cationic dye (methylene blue) from water using polyaniline nanotubes base, J. Phys. Chem. C., 114 (2010) 14377–14383.
[45] R. Jamal, L. Zhang, M. Wang, Q. Zhao, T. Abdiryim, Synthesis of poly (3, 4-propylenedioxythiophene)/MnO_2 composites and their applications in the adsorptive removal of methylene blue, Prog. Nat. Sci. Mater. Int., 26 (2016) 32–40.
[46] V. Vadivelan, K.V. Kumar, Equilibrium, kinetics, mechanism, and process design for the sorption of methylene blue onto rice husk, J. Colloid Interface Sci. 286 (2005) 90–100.
[47] A. Moghimi, A. Mazloumifar, Preconcentration and determination of Mercury (II) from natural water and milk sample by Histidine functionalized multi-walled carbon nanotu bes (MWCNTs-His), African J. Pure Appl. Chem., 7 (2013) 122–130.
[48] Q. Fan, Y. Yang, Y. Hao, X. Zhao, Y. Feng, Preparation of three-dimensional PANI/GO for the separation of Hg (II) from aqueous solution, J. Mol. Liq., 212 (2015) 557–562.
[49] H. Yuan, Z. Hu, X. Liu, H. Tian, R. Li, X. Chang, Solid-phase extraction of Hg (II) on creatine modified activated carbon and determination by ICP-OES in water samples, Int. J. Environ. Anal. Chem., 93 (2013) 1189–1202.
[50] Z. Es' haghi, G.R. Bardajee, S. Azimi, Magnetic dispersive micro solid-phase extraction for trace mercury pre-concentration and determination in water, hemo dialysis solution and fish samples, Microchem. J., 127 (2016) 170–177.
[51] N. Amiri, M.K. Rofouei, J.B. Ghasemi, Multivariate optimization, preconcentration and determination of mercury ions with (1-(p-acetyl phenyl)-3-(o-methyl benzoate)) triaze ne in aqueous samples using ICP-AES, Anal. Methods, 8 (2016) 1111–1119.